

Picosecond thermoelectric dynamics in layered cobaltite thin films probed by terahertz emission spectroscopy

Kouhei Takahashi,* Tsutomu Kanno, Akihiro Sakai, Hiromasa Tamaki, and Yuka Yamada
Materials Research Laboratory, Advanced Research Division, Panasonic Corporation, 3-4 Hikaridai, Seika-cho, Soraku-gun, Kyoto 619-0237, Japan

(Received 12 April 2015; revised manuscript received 27 August 2015; published 28 September 2015)

The operation speed of thermoelectric devices is generally limited to microsecond or millisecond time scales. This is due to the difficulty in manipulating and measuring the thermoelectric transients at high speeds. Although recent advances in optical characterization techniques have succeeded to detect thermoelectric signals in picosecond time scales in a few special nanomaterials such as graphene, thermoelectric dynamics in most of the standard thermoelectric materials still remain unknown. Here we investigate the picosecond carrier dynamics of standard thermoelectric Ca_xCoO_2 thin films by means of terahertz emission spectroscopy. The terahertz radiation signals generated from the Ca_xCoO_2 films by femtosecond laser absorption are found to be strongly dependent on crystal orientation. We discuss that the terahertz emission properties of Ca_xCoO_2 films can be described well in terms of the unique tensorial properties of the Seebeck coefficient. The unordinary terahertz emission property associated with the tensorial property of a Seebeck coefficient provides convincing evidence of picosecond evolution of the thermoelectric current even in this standard material. Our results not only promote general understanding of the ultrafast charge dynamics in solids but may also pave the way to develop optoelectronic devices including bias-free terahertz sources and high-speed infrared sensors.

DOI: [10.1103/PhysRevB.92.094307](https://doi.org/10.1103/PhysRevB.92.094307)

PACS number(s): 78.20.nd, 68.60.Dv, 72.20.Pa, 78.47.—p

I. INTRODUCTION

Thermoelectric (TE) materials have attracted much attention owing to its ability to convert heat directly into electricity and vice versa [1–3]. This has led to development of potential devices such as power generators for waste heat recovery, temperature sensors, and Peltier coolers. However, despite the long history of research in this field, the ultrafast carrier dynamics involved in TE conversion have seldom been studied so far. This is presumably due to the difficulty in detecting the TE diffusion current \mathbf{J}_T at high speeds by standard electronic equipment. Indeed, several attempts have succeeded in measuring nanosecond-TE transients of standard TE materials using a digital oscilloscope and nanosecond laser pulses as a thermal stimulus [4–7]. However, with very few exceptions in special nanomaterials such as graphene [8–10], where the characteristic time scale of carrier thermalization, relaxation, and recombination is much faster than the bulk, it still has been a challenge to characterize the ultrafast TE dynamics in picosecond time resolution.

Meanwhile, terahertz radiation generated by ultrashort laser pulses is known to offer rich information of the nonequilibrium states in solids. Picosecond-charge dynamics can be discussed by identifying the underlying mechanism of terahertz emission. This is known as terahertz emission spectroscopy and its usefulness has been exemplified in various functional materials [11–21]. Recently we have reported generation of terahertz radiation from chalcogenide-semiconductor Bi_2Te_3 thin films, which is known as a typical TE material [22]. The terahertz signal reflected the motion of thermalized charge carriers indicating a picosecond buildup of \mathbf{J}_T . This primary study shed new light in studying the ultrafast TE dynamics by terahertz emission spectroscopy. However, an example on

this single material is not sufficient to argue the generality of ultrafast TE response in a wide variety of materials. To achieve detailed understanding, it is necessary to obtain further supplementary evidences on this issue.

Among various TE materials, the layered cobaltite Ca_xCoO_2 is an attractive candidate for studying the ultrafast carrier dynamics. One of the formidable issues in characterizing the ultrafast TE dynamics by terahertz emission spectroscopy is to distinguish the TE diffusion current from the diffusion current dominated by the photoexcited carriers (the photo-Dember effect). Most of the standard TE materials, including Bi_2Te_3 , is a narrow-gap semiconductor with a carrier concentration of $\sim 10^{19} \text{ cm}^{-3}$. On the other hand, Ca_xCoO_2 is a strongly correlated metal, the carrier concentration of which is about 2–3 orders of magnitude larger than that of Bi_2Te_3 . Owing to this condition, contribution of photoconduction on the laser-induced diffusion current is expected to be negligible for Ca_xCoO_2 . Aside from this aspect, Ca_xCoO_2 is an attractive candidate to examine the ultrafast TE dynamics because it exhibits a unique TE property, which is not normally observed in other TE materials. An unusually large pulsed voltage signal has previously been observed in incline-oriented thin films of Ca_xCoO_2 by heating the film surface with nanosecond laser pulses [6,7]. While the ordinary TE process expects voltage signals to develop parallel to the applied temperature gradient ∇T , it was found that the large voltage transients in the inclined-oriented Ca_xCoO_2 films, which developed parallel to the film surface, were associated with ∇T applied perpendicular to the film surface. This unconventional feature was explained thoroughly by a unique phenomenon called the off-diagonal TE (ODTE) effect which utilizes the off-diagonal term of the Seebeck coefficient tensor \mathbf{S} . Detecting such tensorial property of \mathbf{S} at picosecond time resolution should provide a scientific basis to firmly establish the generality of ultrafast TE response.

*takahashi.kohei@jp.panasonic.com

Here we have employed terahertz emission spectroscopy on Ca_xCoO_2 thin films with different crystal orientations, which exhibit different tensor components of \mathbf{S} . The terahertz emission properties showed strong crystal orientation dependence, which could not be explained by the well-established mechanisms based on photoconduction and nonlinear optical processes. Instead, we discuss that the terahertz emission properties can fully be understood by considering the tensorial property of \mathbf{S} , demonstrating that terahertz emission originates from the TE process. Our results strongly suggest that the TE current develops commonly within ~ 1 ps, which should promote basic understanding of the ultrafast dynamics in TE transport as well as provide renewed opportunity to develop high-speed optoelectronic devices based on TE conversion.

II. EXPERIMENT

Tensorial property of \mathbf{S} is known to appear when a special crystal orientation is realized in anisotropic materials. Figure 1(a) shows the schematic cross-section view of the incline orientation, which is necessary to develop the ODTE effect in Ca_xCoO_2 films. One can notice that the basal- CoO_2 planes of Ca_xCoO_2 are aligned obliquely with respect to the substrate surface [also see the crystal structure of Ca_xCoO_2 in Fig. 1(b)]. According to the theory, the tilted orientation and the anisotropic property of Ca_xCoO_2 arising from its layered structure give rise to a nonzero element in the off-diagonal term of \mathbf{S} . Based on the fundamental formula of the Seebeck effect, $\mathbf{E} = \mathbf{S}\nabla T$ (\mathbf{E} and ∇T being the electric field vector and the temperature gradient vector, respectively), one finds that the off-diagonal component of \mathbf{S} generates a TE field along the film surface (in the x axis) by ∇T applied normal to the film surface (in the z axis), namely $\mathbf{E} \perp \nabla T$ [see the defined laboratory coordinate system in Fig. 1(a)] [6,7]. This

is in contrast to the ordinary Seebeck effect, which utilizes the diagonal component of \mathbf{S} , and thus $\mathbf{E} \parallel \nabla T$.

The samples examined here are 150-nm-thick Ca_xCoO_2 films grown incline oriented on sapphire (11 $\bar{2}$ 3) single crystal substrates by magnetron sputtering. The CoO_2 layers of these films are tilted against the substrate surface at an angle α of 71° , which satisfies the condition necessary for the ODTE effect. For comparison, c axis oriented films with $\alpha = 0^\circ$ were also fabricated on sapphire(0001) substrates. After the film growth, the films were post-annealed at 300°C for 30 min under ozone atmosphere by a UV-asher to supplement oxygen deficiency. The Ca composition x of the films was ~ 0.4 , which was examined by an energy dispersive x-ray analysis. Crystal orientation of the Ca_xCoO_2 films was examined by transmittance electron microscopy (TEM) and four-circle x-ray diffraction (XRD) analysis with $\text{Cu}K\alpha$ radiation. The structural features of the films are summarized in Fig. 2. Further details of film fabrication and characterization are described in Ref. [23].

For terahertz emission spectroscopy, a single pair of Au metal electrodes with 150 nm thickness and $0.3 \text{ mm} \times 2 \text{ mm}$ in dimension was fabricated on the Ca_xCoO_2 film surface. The electrode pair was separated along the x axis by $100 \mu\text{m}$. The role of Au electrodes is twofold, (i) to enhance terahertz emission via antenna effect and/or dipole quenching and (ii) to measure steady-state TE voltages induced by laser heating. Note that the films were unbiased throughout the entire measurement. A mode-locked Ti:sapphire laser with center wavelength of 800 nm, repetition rate of 80 MHz, and pulse duration of 100 fs was used as the laser source to generate terahertz radiation. The laser beam, which was focused to a diameter of $150 \mu\text{m}$, was illuminated on the Ca_xCoO_2 film surface at normal incidence. The generated terahertz radiation was detected in a transmission geometry by a photoconductive sampling technique using a low-temperature grown GaAs (LT-GaAs) photoconductive antenna as a terahertz detector [24]. This method enables polarization-sensitive detection of terahertz radiation, which detects only the terahertz field \mathbf{E}_{THz} component parallel to the x axis.

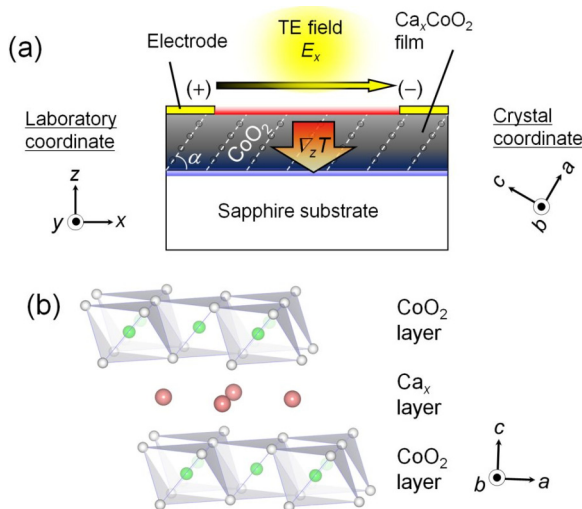


FIG. 1. (Color online) (a) Schematic cross section of the incline-oriented Ca_xCoO_2 film to describe the ODTE effect. The TE field develops parallel to the film surface by applying ∇T perpendicular to the film surface. (b) Layered crystal structure of Ca_xCoO_2 . Insulating Ca_x layers are sandwiched by the conductive CoO_2 layers giving rise to an anisotropic physical property.

III. RESULTS

A. Terahertz emission properties of Ca_xCoO_2 films

The classical Maxwell's equations describe that a time varying current \mathbf{J} in a subpicosecond time scale generates terahertz radiation determined by the following relationship: $\mathbf{E}_{\text{THz}} \propto \partial \mathbf{J} / \partial t$, where t is time. This formula not only describes that the frequency of \mathbf{E}_{THz} depends on the rise time of \mathbf{J} , but also describes that the polarization and polarity of \mathbf{E}_{THz} depend on the orientation of source \mathbf{J} . In general, to generate terahertz radiation by femtosecond laser illumination, it usually requires some kind of broken inversion symmetry across the area excited by the laser beam. This is because the charges excited by the laser need to move asymmetrically in order to create net \mathbf{J} .

In Fig. 3(a) we summarize the terahertz time-domain waveforms of the incline-oriented Ca_xCoO_2 film generated by focusing the laser beam on three different positions around the $\text{Au}/\text{Ca}_x\text{CoO}_2/\text{Au}$ contacts, i.e., (i) laser beam focused

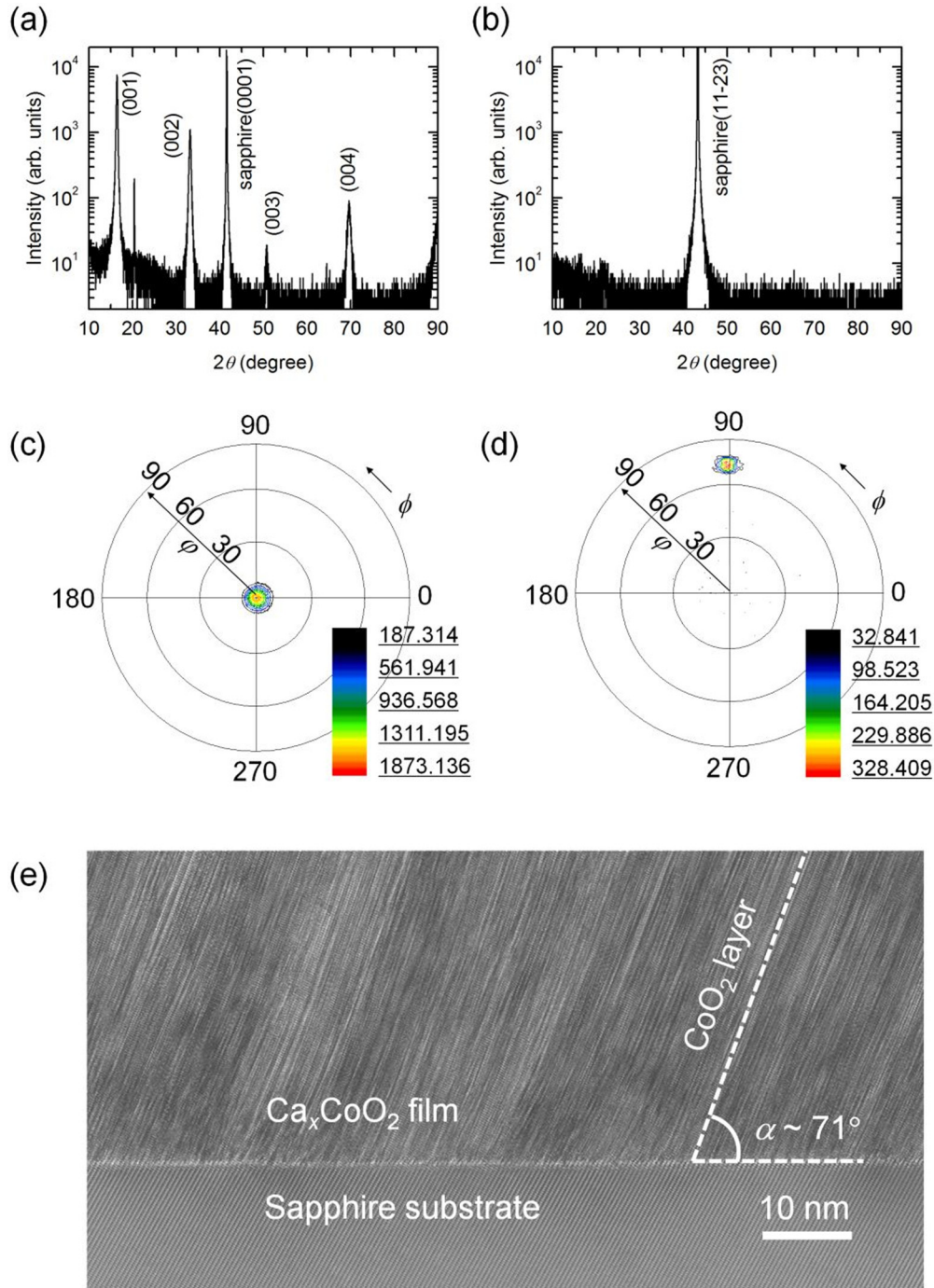


FIG. 2. (Color online) θ - 2θ scan XRD pattern of (a) c axis oriented Ca_xCoO_2 film and (b) incline-oriented Ca_xCoO_2 film grown on sapphire(0001) and sapphire(11-23) substrate, respectively. The absence of Ca_xCoO_2 diffraction peaks in (b) reflects the incline orientation of Ca_xCoO_2 . Pole-figure XRD pattern of (c) c axis oriented film and (d) incline-oriented film probing the (001) orientation of Ca_xCoO_2 . The (001) peak observed at $\psi = 0^\circ$ in (c) represents that the basal- CoO_2 layers are aligned parallel to the substrate surface. The (001) peak observed at $\psi = 71^\circ$ in (d) represents that the CoO_2 layers are aligned tilted by this angle with respect to the substrate surface. (e) TEM image of the incline-oriented Ca_xCoO_2 film. The tilted stripes in the Ca_xCoO_2 film correspond to the CoO_2 layers.

symmetrically across the Au/ Ca_xCoO_2 /Au contacts, (ii) laser beam focused asymmetrically across the left Au/ Ca_xCoO_2 contact (Au layer on the left-side half of the laser-covered area), and (iii) laser beam focused asymmetrically across the right Ca_xCoO_2 /Au contact (Au layer on the right-side half of the laser-covered area) [see the inset in Fig. 3(a)]. Note

that the amplitude of terahertz radiation is described with the output signal of the lock-in amplifier (unit in volts). Despite the difference in spatial symmetry of the laser-excited area, positive pulse signals, with a duration of no more than few picoseconds, were commonly observed for all three cases. Fourier transformed power spectrum of these short-duration

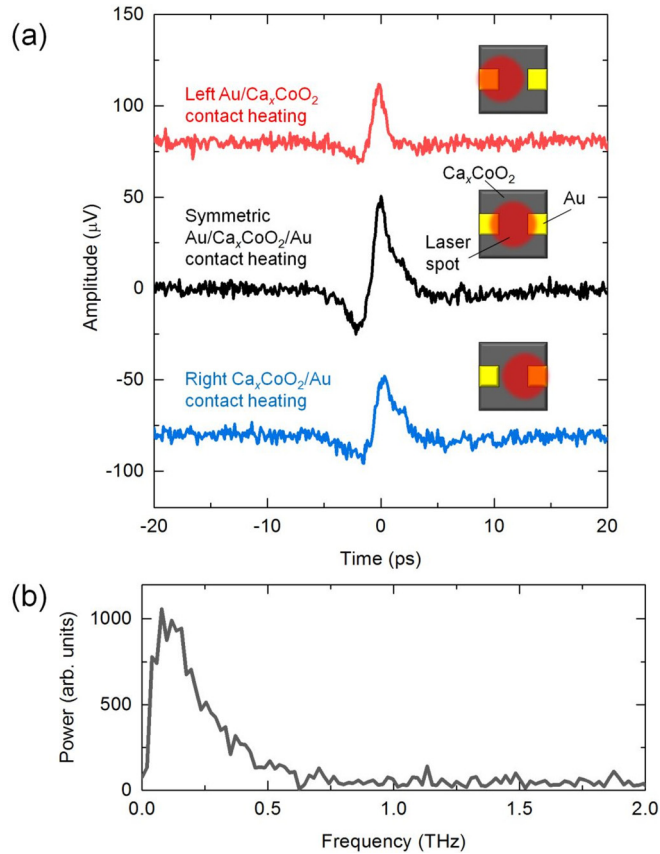


FIG. 3. (Color online) (a) Terahertz time-domain waveforms of an incline-oriented Ca_xCoO_2 film generated by focusing the laser beam on three different positions around the $\text{Au}/\text{Ca}_x\text{CoO}_2/\text{Au}$ contacts as follows: (i) laser beam focused symmetrically across the $\text{Au}/\text{Ca}_x\text{CoO}_2/\text{Au}$ contacts, (ii) laser beam focused asymmetrically across the left $\text{Au}/\text{Ca}_x\text{CoO}_2$ contact (Au layer on the left-side half of the laser-covered area), and (iii) laser beam focused asymmetrically across the right $\text{Ca}_x\text{CoO}_2/\text{Au}$ contact (Au layer on the right-side half of the laser-covered area). The inset shows the schematic of the laser position on the $\text{Au}/\text{Ca}_x\text{CoO}_2/\text{Au}$ contact used to measure each waveform. Note that the waveforms are vertically offset for clarity and that the amplitude is expressed by the output signal of the lock-in amplifier. (b) Fourier transformed power spectrum of the terahertz waveform generated by focusing the laser beam symmetrically across the $\text{Au}/\text{Ca}_x\text{CoO}_2/\text{Au}$ contacts.

pulses exhibited frequency components up to 0.6 THz [see Fig. 3(b)]. This indicates that net \mathbf{J} is introduced within a similar fast time scale by the laser stimulus.

Meanwhile, it is interesting to find that a same “positive” pulse is seen in the time-domain waveform regardless of which part of the $\text{Au}/\text{Ca}_x\text{CoO}_2/\text{Au}$ contact is excited by the laser beam. This represents that \mathbf{J} created by laser illumination in the incline-oriented film is directed in the same direction with the same polarity in spite of the difference in local spatial symmetry of the laser-excited area. This is in contrast to the features of terahertz radiation generated via the second order nonlinear optical effect known as optical rectification (OR). The centrosymmetric crystal structure of Ca_xCoO_2 (space group of $C2/m$) supports this aspect, in which the even order nonlinear optical process is

forbidden. In our series of measurement, we found that terahertz emission was not detectable when the laser spot did not cross any of the $\text{Au}/\text{Ca}_x\text{CoO}_2/\text{Au}$ boundaries. This implies the importance of metallic Au films for terahertz emission from the Ca_xCoO_2 film. Previous studies on photoconductive semiconductors have shown that terahertz emission could greatly be enhanced by the presence of metallic contacts via an antenna effect or dipole quenching [25–28]. We assume that similar enhancement effect by metal contacts plays an essential role in terahertz radiation from the $\text{Au}/\text{Ca}_x\text{CoO}_2/\text{Au}$ contact.

Other than nonlinear polarization, photoexcited carriers usually have an important part in terahertz emission either via drift or diffusion current. Since the Ca_xCoO_2 film is unbiased throughout the measurement, drift current can only originate from carrier acceleration by a built-in electric field [25,29,30]. Indeed, surface depletion field or Schottky depletion field may be present at the $\text{Au}/\text{Ca}_x\text{CoO}_2$ contact in our sample. However, the polarity of the built-in field would be inverted for an inverted $\text{Au}/\text{Ca}_x\text{CoO}_2$ symmetry, and hence, the resulting drift photocurrent as well [25]. As mentioned above, an opposite flow of \mathbf{J} would induce \mathbf{E}_{THz} with a reversed phase. This means that polarity of \mathbf{E}_{THz} driven via the built-in electric field should reflect the spatial symmetry of the laser-excited area, which is not the case for the incline-oriented Ca_xCoO_2 film. On the other hand, photo-Dember effect is a typical mechanism for terahertz emission dominated by diffusion current. In this mechanism, photoexcited electrons and holes diffusing in the same directions, but in different speeds, create net \mathbf{J} . One may notice that the present sample configuration is in analogy with the lateral photo-Dember devices [26–28]. However, even in the photo-Dember mechanism, \mathbf{E}_{THz} should show reversed phases for an inverted $\text{Au}/\text{Ca}_x\text{CoO}_2$ symmetry, and also, absence of terahertz emission when the $\text{Au}/\text{Ca}_x\text{CoO}_2/\text{Au}$ contact is excited symmetrically. This is again in contrast to the feature in Fig. 3(a), which eliminates the possibility of diffusion “photocurrent” as the source of terahertz emission in the incline-oriented Ca_xCoO_2 film.

The main subject of discussion here is thus to identify the origin of in-plane \mathbf{J} induced by laser illumination, the polarity of which is hardly influenced by the spatial symmetry of the laser-excited area. As we discuss below, the results in Fig. 3(a) seems reasonable if we consider the issue in terms of the TE effect. To achieve insight, we have simultaneously measured the laser-induced voltage V_{laser} that develops between the Au electrodes in steady state during the terahertz emission measurement. Here we especially focus on the case for which the laser beam is symmetrically illuminated across the $\text{Au}/\text{Ca}_x\text{CoO}_2/\text{Au}$ contacts. Normally, when \mathbf{S} is treated as a scalar (when the off-diagonal term of \mathbf{S} is zero), symmetric surface heating between two metal contacts on a TE material does not create a measurable TE voltage between the metal contacts. This is because symmetric heating creates no net ∇T along the surface. However, in the incline-oriented Ca_xCoO_2 films, in which the off-diagonal terms of \mathbf{S} become nonzero, it has been reported that in-plane V_{laser} can be generated via the ODTE effect even by symmetric surface heating. This has been demonstrated in the incline-oriented Ca_xCoO_2 films by using various light sources as thermal stimuli [6,7,31]. The in-plane V_{laser} was confirmed to be associated with ∇T applied normal

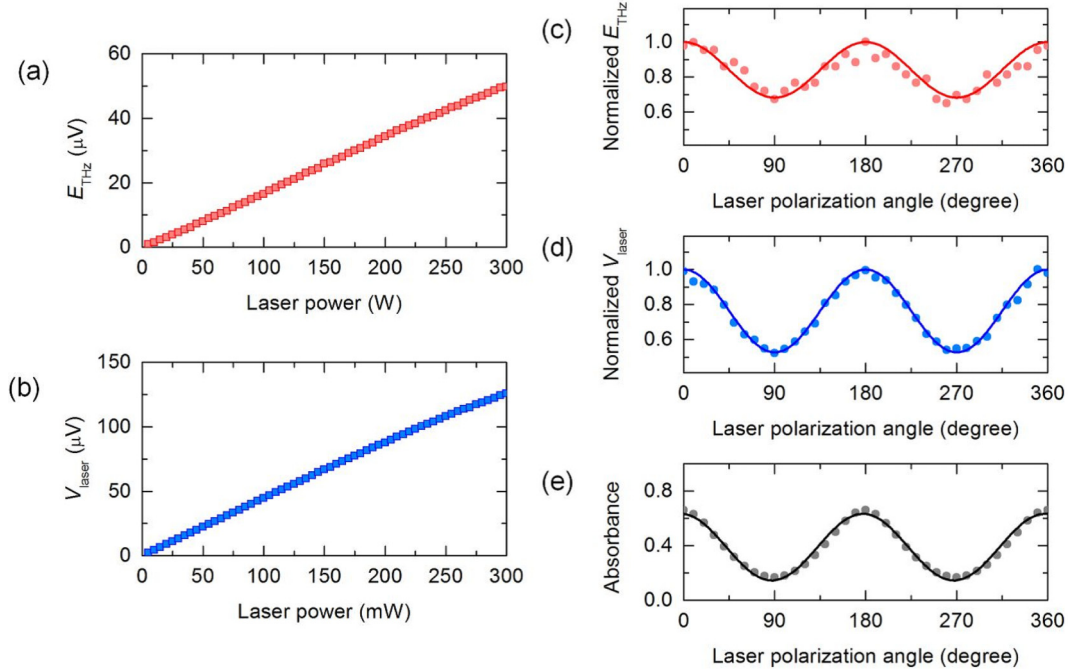


FIG. 4. (Color online) Laser power dependence of (a) E_{THz} and (b) V_{laser} of the incline-oriented Ca_xCoO_2 film measured by focusing the laser beam symmetrically across the $\text{Au}/\text{Ca}_x\text{CoO}_2/\text{Au}$ contacts. Note that volt unit of E_{THz} derives from the output signal of a lock-in amplifier. Laser polarization dependence of (c) E_{THz} , (d) V_{laser} , and (e) A measured at a fixed laser power. E_{THz} and V_{laser} are normalized by the maximum values for clarity. The solid lines are sinusoidal fits to the data.

to the film surface, which agreed well with the feature of the ODTE effect.

In the present work we found that E_{THz} and V_{laser} behave similarly under various laser conditions. Figures 4(a) and 4(b) show the laser power P_{laser} dependence of E_{THz} and V_{laser} , respectively, measured by focusing the laser beam symmetrically on the $\text{Au}/\text{Ca}_x\text{CoO}_2/\text{Au}$ contact. We see that both quantities increase linearly with increasing P_{laser} . The linear increase in V_{laser} with increasing P_{laser} is reasonable given that V_{laser} is driven by the ODTE effect. This is because \mathbf{E} via the ODTE effect scales linearly with $\nabla\mathbf{T}$ applied normal to the film surface, which scales linearly with the amount of laser absorption. We have also measured the laser polarization dependence of E_{THz} and V_{laser} at a fixed P_{laser} . Figures 4(c) and 4(d) show E_{THz} and V_{laser} measured as a function of the angle ϕ between the laser polarization plane and the spatial y axis. Thus, $\phi = 0^\circ$ and 90° corresponds to $\mathbf{E}_{\text{light}} \parallel y$ and $\mathbf{E}_{\text{light}} \parallel x$, respectively, where $\mathbf{E}_{\text{light}}$ is the electric field vector of the laser light. Both E_{THz} and V_{laser} show a sinusoidal dependence on ϕ with a maximum at 0° and a minimum at 90° . We also show in Fig. 4(e) the laser absorbance A of the incline-oriented film measured as a function of ϕ . We see that A , which is a measure of laser absorption, also varies sinusoidally with a same phase as the other two curves. Such anisotropy in laser absorption is consistent with the anisotropic dc transport property of this material, i.e., a metallic conduction is observed in the ab planes while semiconductive conduction is observed along the c axis [32]. The ϕ dependence of A thus describes the ϕ dependence of V_{laser} well in terms of the ODTE effect, and also for the ϕ dependence of E_{THz} , if the two quantities were to stem from the same mechanism.

For a structure shown in Fig. 1(a), the tensor components of \mathbf{S} can be described as [31]

$$\mathbf{S} = \begin{bmatrix} S_{xx} & S_{xz} \\ S_{zx} & S_{zz} \end{bmatrix} = \begin{bmatrix} S_{ab} \cos^2 \alpha + S_c \sin^2 \alpha & \frac{1}{2}(S_{ab} - S_c) \sin 2\alpha \\ \frac{1}{2}(S_{ab} - S_c) \sin 2\alpha & S_c \cos^2 \alpha + S_{ab} \sin^2 \alpha \end{bmatrix}. \quad (1)$$

Note that S_{ab} and S_c represents S in the ab plane and the c axis, respectively. We also note that components in the xy plane and the yz plane are not shown for simplicity since they do not play an essential role in any of the discussion here. In Eq. (1), one can see that the off-diagonal term S_{xz} and S_{zx} becomes nonzero when the material simultaneously satisfies $S_{ab} \neq S_c$ and $\alpha \neq 0^\circ, 90^\circ$. This is indeed the case for the incline-oriented Ca_xCoO_2 film examined here [32]. The vector components of the TE field $\mathbf{E} [= (E_x, E_z)]$ via the Seebeck effect can be deduced from the tensor product of \mathbf{S} and $\nabla\mathbf{T} [= (\nabla_x T, \nabla_z T)]$ as

$$\mathbf{E} = \begin{bmatrix} E_x \\ E_z \end{bmatrix} = \begin{bmatrix} S_{xx} \nabla_x T + S_{xz} \nabla_z T \\ S_{zx} \nabla_x T + S_{zz} \nabla_z T \end{bmatrix}. \quad (2)$$

From Eq. (2) E_x is given by the form $S_{xx} \nabla_x T + S_{xz} \nabla_z T$. As we explained above, symmetric surface heating by laser would induce a symmetric in-plane temperature distribution, which would result in no net $\nabla_x T$ ($\nabla_x T = 0$). However, even by symmetric surface heating, $\nabla_z T$ still survives, and therefore, creates E_x of $S_{xz} \nabla_z T$. We can then understand the presence of an in-plane TE component even by symmetric heating of the $\text{Au}/\text{Ca}_x\text{CoO}_2/\text{Au}$ contact in the incline-oriented film. This in-plane TE component associated with $\nabla_z T$ is

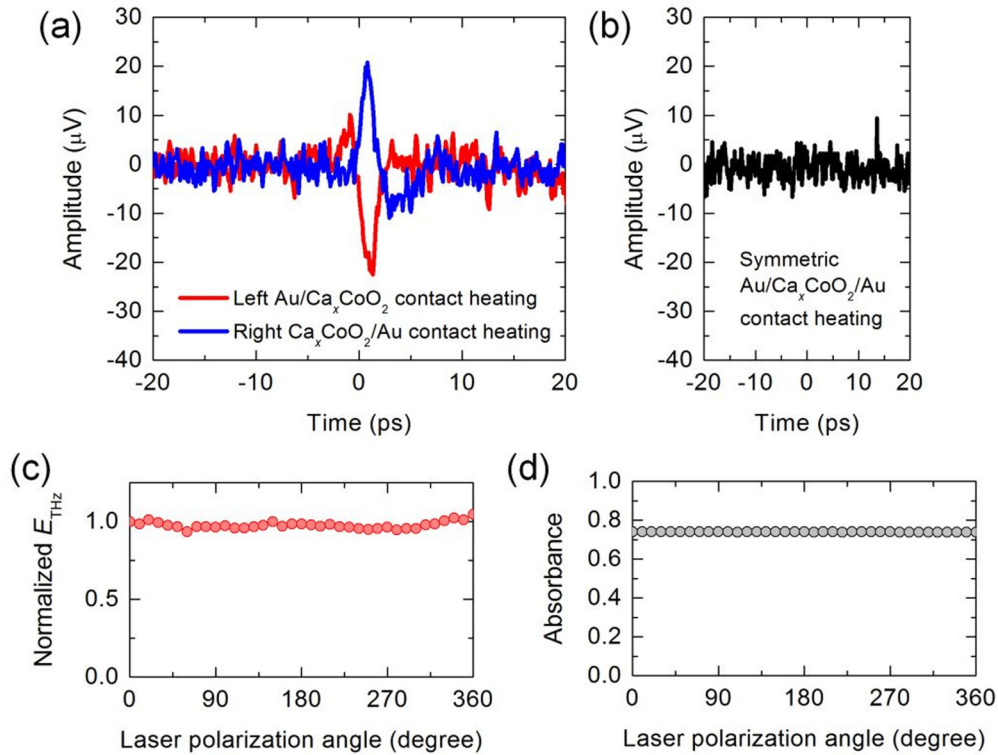


FIG. 5. (Color online) Time-domain terahertz waveforms of c axis oriented Ca_{*x*}CoO₂ film generated by focusing the laser beam (a) asymmetrically across the left Au/Ca_{*x*}CoO₂ contact (Au layer on the left-side half of the laser-covered area) and the right Ca_{*x*}CoO₂/Au contact (Au layer on the right-side half of the laser-covered area), and (b) symmetrically across the Au/Ca_{*x*}CoO₂/Au contacts. Note that the laser beam is focused down to a diameter of 50 μm to increase the laser intensity to clarify the peak structure in (b). Laser polarization dependence of (c) E_{THz} and (d) A measured at a fixed laser power. E_{THz} is normalized by the maximum values for clarity.

presumably related to the terahertz radiation property of the incline-oriented film, which is hardly affected by the spatial symmetry of the laser-excited area.

To further validate that terahertz emission from the Ca_{*x*}CoO₂ films is related to the Seebeck effect, we have examined terahertz emission from a c axis oriented Ca_{*x*}CoO₂ film, which corresponds to $\alpha = 0^\circ$. According to Eq. (1), only the diagonal components of \mathbf{S} become available in Ca_{*x*}CoO₂ films with $\alpha = 0^\circ$. In this case, the in-plane TE component E_x will be expressed as $S_{xx}\nabla_x T$ because $S_{xz} = 0$ [also see Eq. (2)]. By focusing the laser beam either on the left Au/Ca_{*x*}CoO₂ contact or the right Ca_{*x*}CoO₂/Au contact, we can create net $\nabla_x T$ directing in the opposite directions between the two Au electrodes. This would then create E_x directing oppositely as well. Figures 5(a) and 5(b) show the terahertz waveforms generated from a c axis oriented Ca_{*x*}CoO₂ film, which was grown on a sapphire(0001) substrate. Au film electrodes were fabricated on the Ca_{*x*}CoO₂ surface as in the case of the incline-oriented film. As expected above, we see a clear phase reversal of E_{THz} by the left Au/Ca_{*x*}CoO₂ contact heating and the right Ca_{*x*}CoO₂/Au contact heating. Moreover, by symmetric laser excitation of the Au/Ca_{*x*}CoO₂/Au contact, which would create no net $\nabla_x T$ (and no net E_x), we see no significant peak structure in the time-domain waveform. These features are consistent with the photoinduced TE effect characterized at much slower time resolutions [6,31]. We also show in Figs. 5(c) and 5(d) the ϕ dependence of E_{THz} and A , respectively, of the c axis oriented film. Reflecting the

isotropic transport property within the CoO₂ planes, A of the c axis oriented film does not show any ϕ dependence. Similarly, E_{THz} is also independent to ϕ , which is in contrast to the feature of OR, but is reasonable from a TE point of view.

B. Thermoelectric transport model

The terahertz emission properties associated with the tensorial property of \mathbf{S} clearly demonstrate the direct relation between terahertz emission and the Seebeck effect. In terms of TE conversion, two different models can be proposed to describe the mechanism of terahertz emission from the Ca_{*x*}CoO₂ films.

The first model considers a drift current \mathbf{J}_D as the source of terahertz emission [see the schematic in Fig. 6(a)]. As explained above, steady-state TE voltage develops between the two Au electrodes in the Ca_{*x*}CoO₂ film even by femtosecond laser pulse heating. This is because the film temperature raised by the first laser pulse does not completely relax to the original temperature by the arrival of the next laser pulse, which creates a weak steady-state ∇T . Note that the repetition rate of the laser pulse is 80 MHz (the pulse interval is 12.5 ns), while the thermal relaxation rate of the 150-nm-thick Ca_{*x*}CoO₂ film is ~ 20 ns [7]. If femtosecond laser absorption were to abruptly create additional photoexcited carriers by interband transition, this steady-state TE field would instantly create a photo- \mathbf{J}_D by acceleration of the photoexcited carriers. This

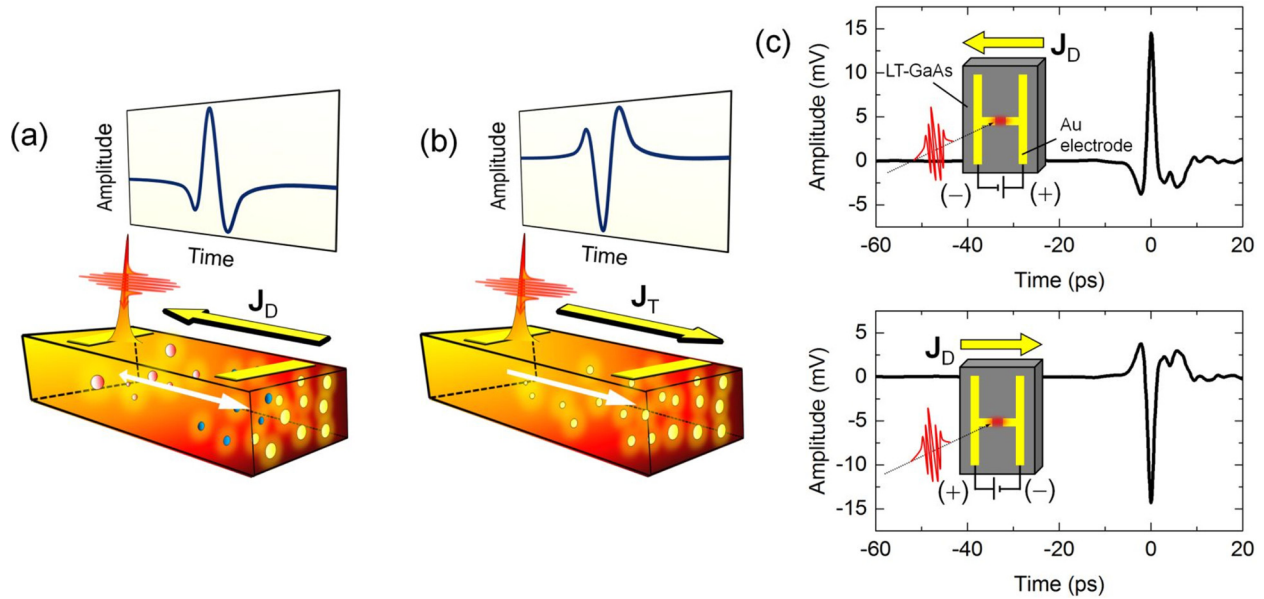


FIG. 6. (Color online) Schematic of the TE transport model to describe terahertz emission from Ca_xCoO_2 films. (a) A model in which terahertz emission is governed by \mathbf{J}_D . In this model, \mathbf{J}_D is associated with the photoexcited carriers accelerated by a steady-state TE field. (b) A model in which terahertz emission is governed by \mathbf{J}_T . In this mode, \mathbf{J}_T is associated with diffusion of thermalized holes. Yellow spheres represent conduction holes, whereas the blue and the red spheres represent photoexcited electrons and holes, respectively. The expected peak sign of \mathbf{E}_{THz} is also shown for each model under left Au/ Ca_xCoO_2 contact heating in c axis oriented film. (c) Terahertz waveform generated from LT-GaAs photoconductive emitter by applying bias voltage of +5 V and -5 V (left electrode grounded). The result manifests that current flowing from right to left (left to right) generates terahertz radiation with a positive (negative) peak signal in the present optical setup.

can generate a terahertz radiation given by the following relationship: $\mathbf{E}_{\text{THz}} \propto \partial \mathbf{J}_D / \partial t$.

The second model considers diffusion of hot carriers associated with ∇T , namely \mathbf{J}_T , as the source of terahertz emission [see the schematic in Fig. 6(b)]. The Seebeck effect occurs by the diffusion of charge carriers associated with ∇T so as to compensate for the difference in average energy of conduction electrons/holes between areas of different temperatures. In the initial stage of Seebeck effect, carriers start to diffuse away from the heated area to the cooler part of the material. This process corresponds to the rise in \mathbf{J}_T . In the next step, diffusion of hot carriers results in charge accumulation at the cooler side of the material. The accumulated charges then create a repulsion force for the incoming hot carriers, which eventually suppresses \mathbf{J}_T to zero. The second model assumes that this transient \mathbf{J}_T , rather than \mathbf{J}_D , generates terahertz radiation given by the following relationship: $\mathbf{E}_{\text{THz}} \propto \partial \mathbf{J}_T / \partial t$.

To examine the availability of these models, we have measured terahertz emission from a standard voltage-biased LT-GaAs photoconductive emitter. This measurement provides us the relation between the polarity of \mathbf{E}_{THz} and the direction of the source \mathbf{J} in the present optical setup. In a LT-GaAs photoconductive switch, photoexcited carriers are accelerated by an external bias field applied between a pair of metal electrodes. This creates a transient photo- \mathbf{J} that serves as the source of terahertz emission. Figure 6(c) shows two terahertz waveforms generated from a LT-GaAs photoconductive switch by applying an external bias voltage of ± 5 V (the left electrode grounded). Reflecting the reverse bias field (and reverse photo- \mathbf{J}), we see that the two terahertz waveforms show opposite phase signs. An important aspect provided by this

measurement is that \mathbf{J} flowing from right to left in the present optical setup induces \mathbf{E}_{THz} with a positive pulse, whereas that flowing from left to right induces \mathbf{E}_{THz} with a negative pulse [see the inset of Fig. 6(c)].

We first judge the possibility of the first model based on the above-mentioned relation between the polarity of \mathbf{E}_{THz} and the direction of \mathbf{J} . Since Ca_xCoO_2 is a p -type material, positively charged holes act as the majority carriers that play a dominant role in TE conversion. For the c axis oriented film, laser illumination on the left Au/ Ca_xCoO_2 contact would increase the local temperature of this region with respect to the right $\text{Ca}_x\text{CoO}_2/\text{Au}$ contact. This situation would then lead to accumulation of holes on the right Au electrode by the Seebeck effect. Namely, the TE field would be directing from right to left in this situation. \mathbf{J}_D created by this steady-state TE field would then be directing from right to left as well, which should generate \mathbf{E}_{THz} with a positive pulse based on the first model [see the schematic in Fig. 6(a)]. The phase sign of \mathbf{E}_{THz} would be the opposite for right $\text{Ca}_x\text{CoO}_2/\text{Au}$ contact heating. However, the phase signs of \mathbf{E}_{THz} of the c axis oriented Ca_xCoO_2 film in Fig. 5(a) disagree with those suggested above. Peak sign of \mathbf{E}_{THz} of the incline-oriented film also disagrees with that expected from this model. These features exclude the possibility of \mathbf{J}_D as the source of terahertz emission in the Ca_xCoO_2 films.

On the other hand, the second model provides a decent explanation for the terahertz emission properties of the Ca_xCoO_2 films. For the c axis oriented film, laser illumination on the left Au/ Ca_xCoO_2 contact induces diffusion of hot holes towards the right $\text{Ca}_x\text{CoO}_2/\text{Au}$ contact via the Seebeck effect, which creates \mathbf{J}_T directing from left to right. In the same

manner, right $\text{Ca}_x\text{CoO}_2/\text{Au}$ contact laser heating would create \mathbf{J}_T directing from right to left. If we consider \mathbf{J}_T as the source of terahertz emission, we expect to see \mathbf{E}_{THz} with a negative peak for left $\text{Au}/\text{Ca}_x\text{CoO}_2$ contact laser heating, whereas a positive peak for right $\text{Ca}_x\text{CoO}_2/\text{Au}$ contact laser heating [see the schematic in Fig. 6(b)]. The experimental phase sign of \mathbf{E}_{THz} of the c axis oriented film in Fig. 5(a) is indeed consistent with the above-mentioned description. In addition, the positive peak of \mathbf{E}_{THz} observed in the incline-oriented film [Fig. 3(a)] also agrees with the behavior expected in this model.

IV. DISCUSSION

We further discuss the availability of the TE model in terms of magnitude. Under ultrashort laser heating, contribution of $\nabla_z T$ on E_x is much more dominant over $\nabla_x T$ in the incline-oriented film. Namely, the influence of the ODTE effect is much greater than the ordinary TE effect under laser heating. This is because an increase in temperature decays rapidly in the z axis within several hundred nanometers depending on the laser penetration depth of Ca_xCoO_2 , whereas that in the x axis decays rather moderately within several ten micrometers depending on the laser beam size. Thus, E_x by laser heating in the incline-oriented film will be given by $\sim S_{xz} \nabla_z T$ (contribution of $\nabla_x T$ can be neglected) [also see Eq. (2)]. Meanwhile, \mathbf{J}_T associated with the Seebeck effect (the TE current) is given by $\sigma \nabla T$, where σ is the electrical conductivity tensor. Note that σ can be described by the same transport tensor as in Eq. (1) by substituting S by σ . By expanding $\sigma \nabla T$ into each component, one can find that $\nabla_z T$ would create an in-plane \mathbf{J}_T , J_{Tx} , of $(\sigma_{xx} S_{xz} + \sigma_{xz} S_{zz}) \nabla_z T$ by the ODTE effect. On the other hand, J_{Tx} of the c axis oriented film is given by $\sigma_{xx} S_{xx} \nabla_x T$. In the TE transport model, we expect \mathbf{E}_{THz} to scale linearly with $\partial \mathbf{J}_T / \partial t$. Based on \mathbf{S} and σ of Ca_xCoO_2 , we have compared the magnitude of J_{Tx} expected between the incline-oriented film and the c axis oriented film. We found that the magnitude of J_{Tx} of the incline-oriented film should be about 25 times larger than that of the c axis oriented film under the same laser condition. On the other hand, the ratio of E_{THz} between the two types of films were actually about 7–12 depending on samples. We assume that this deviation is within the acceptable range considering that static physical properties were used for the estimation of J_{Tx} [32], and also, assuming a probable difference in crystalline quality between the two types of films.

This model is also valid in terms of time scale. In doped semiconductors and metals, femtosecond laser absorption creates additional numbers of photoexcited carriers as well as excites free carriers to higher energies (create hot carriers). The carriers are then redistributed throughout the band by carrier-carrier scattering and carrier-phonon scattering, transferring their energy to other carriers and the crystal lattice. The two processes occur simultaneously, but the carriers reach equilibrium sooner than the lattice, which is when the carrier distribution is described by a Fermi-Dirac distribution. This is also when a carrier temperature T_e can be defined. Although it requires alternative optical studies to identify the precise carrier scattering rate of Ca_xCoO_2 , this time scale is typically known to be in the order of subpicoseconds [33]. On the other hand, the lattice normally completes heating several picoseconds after the arrival of the laser pulse with less

increase than T_e . At this stage, the initially raised T_e is cooled down to the lattice temperature T_L , where thermal equilibrium is reached. After this stage we could not decouple T_e and T_L . The two temperatures then gradually decrease towards the original state at the same rate by transferring the excess energy to the underlying substrate (~ 20 ns for the 150-nm-thick Ca_xCoO_2 film). The nonequilibrium dynamics in Ca_xCoO_2 films upon femtosecond laser heating can be described as such. Meanwhile, it is noteworthy that the Seebeck coefficient is defined as the difference between the average energy of carriers and the Fermi energy. Since the average energy of carriers is defined by T_e , the TE process should reflect the changes in T_e as well. As we explained above, T_e is expected to show abrupt increase and decrease within the first few picoseconds by femtosecond laser absorption, followed by a gradual decrease within several 10 ns. The ~ 1 ps rise of the electromagnetic pulse observed in this study shows good agreement with the expected rise time of \mathbf{J}_T , which should be slightly delayed from the rise time of T_e .

According to the previous spectroscopic studies on a family-compound Na_xCoO_2 [34,35], the photon energy of the laser pulse used here (1.55 eV) corresponds to the energy scale at which two types of optical transition can occur, i.e., (i) transition from the partially filled Co $3d t_{2g}$ band to the empty Co $3d e_g$ band, and (ii) transition from the filled O $2p$ to the partially filled Co $3d t_{2g}$ band. In these class of layered cobaltites, holes supplied from the partially filled Co $3d t_{2g}$ band serve as the charge carriers, thus contributing to the hole Fermi surface. The $t_{2g} \rightarrow e_g$ transition thus corresponds to transition from the hole valence band to the hole conduction band, which creates an additional number of photoexcited carriers. On the other hand, the O $2p \rightarrow t_{2g}$ transition corresponds to the transition between two different hole conduction bands, which increases the energy of the conduction holes without altering their total number. For $\mathbf{E}_{\text{light}} \perp c$ excitation, both types of transition are expected to take part in the absorption process. However, for $\mathbf{E}_{\text{light}} \parallel c$, the O $2p \rightarrow t_{2g}$ transition should be much weaker given the semiconductive nature of the c axis transport, and hence, absence of hole Fermi surface along this direction. This is indeed reflected in the anisotropic A in the incline-oriented film, where large absorbance is observed at $\mathbf{E}_{\text{light}} \parallel y$ compared to that at $\mathbf{E}_{\text{light}} \parallel x$ [see Fig. 4(e)]. The large absorbance, as well as the large E_{THz} , at $\mathbf{E}_{\text{light}} \parallel y$ thus indicates that O $2p \rightarrow t_{2g}$ transition has substantial contribution over the $t_{2g} \rightarrow e_g$ transition for absorption at 1.55 eV, and for the terahertz emission process in the Ca_xCoO_2 films. To achieve further insight, we had measured the electrical resistance R between the Au electrodes to examine the influence of photoexcited carriers on the transport property of the Ca_xCoO_2 film. In general, laser absorption in semiconductors or insulators results in photoconductivity, which is represented by the large reduction in R . In fact, in LT-GaAs photoconductive switch, which was used as a reference terahertz emitter, R reduces dramatically from 10^9 to $10^5 \Omega$ under the laser condition used to generate terahertz radiation. On the other hand, we confirmed that R of Ca_xCoO_2 hardly changed under the laser condition used to generate terahertz radiation in the present work. These aspects support the TE transport model, where \mathbf{J}_T is governed by the motion of majority carriers rather than the photoexcited carriers.

V. CONCLUSION

The terahertz emission properties of Ca_xCoO_2 films demonstrated here strongly supports that the Seebeck effect takes place in picosecond time scales even in standard TE materials. The results shown here not only promote fundamental understanding of ultrafast physics of solids, but may also stimulate development of ultrafast TE devices utilizing the ODTE effect. The photo-TE signal by the ODTE effect makes use of the large ∇T applied normal to the film surface. This leads to a higher photoresponse for the ODTE effect over the ordinary TE effect. Other than Ca_xCoO_2 , Bi is another example that exhibits the ODTE effect. \mathbf{J}_T driven by the ODTE effect is known to be roughly proportional to the following three components: (i) σ_{ab} ($= 1/\rho_{ab}$, where ρ_{ab} is electrical resistivity along the ab plane), (ii) ΔS ($= S_{ab} - S_c$), and (iii) the laser penetration depth l (inverse of the absorption coefficient) which determines $\nabla_z T$. If we compare these values between Ca_xCoO_2 and Bi, σ_{ab} is ~ 15 times larger for Bi (ρ_{ab} of Bi and Ca_xCoO_2 is

0.1 and 1.5 $\text{m}\Omega\text{cm}$, respectively [32,36]), ΔS is ~ 1.4 times larger for Bi (ΔS of Bi and Ca_xCoO_2 is 50 and 35 $\mu\text{V}/\text{K}$, respectively [32,37]), and l is ~ 7 times larger for Bi (l of Bi and Ca_xCoO_2 is 29 and 93 nm, respectively [38]). $\sigma_{ab}\Delta S\nabla_z T$ of Bi is then larger than that of Ca_xCoO_2 by a factor of ~ 70 . Furthermore, by optimizing α to 45° , the photo-ODTE response of the incline-oriented Bi film can be 100 times larger than that of the incline-oriented Ca_xCoO_2 film examined here. Indeed, the high σ of Bi may result in lower transmittance in terahertz radiation, and therefore, the terahertz intensity may not directly reflect the increase in $\sigma_{ab}\Delta S\nabla_z T$. Nevertheless, the above-mentioned feature suggests that the incline-oriented Bi films, when they are designed optimally for terahertz emitters, have a great chance of showing comparable intensity to the voltage-biased LT-GaAs photoconductive switch. The large and the ultrafast photo-TE response provided by the ODTE effect thus sets expectations to future development of various ultrafast optoelectronic devices such as bias-free terahertz emitters and bolometers with picosecond time resolution.

-
- [1] G. J. Snyder and E. S. Toberer, *Nat. Mater.* **7**, 105 (2008).
 [2] F. J. DiSalvo, *Science* **285**, 703 (1999).
 [3] L. E. Bell, *Science* **321**, 1457 (2008).
 [4] Th. Zahner, R. Stierstorfer, S. Reindl, T. Schauer, A. Penzkofer, and H. Lengfellner, *Physica C* **313**, 37 (1999).
 [5] X. H. Li, H.-U. Habermeier, and P. X. Zhang, *J. Magn. Magn. Mater.* **211**, 232 (2000).
 [6] K. Takahashi, T. Kanno, A. Sakai, H. Adachi, and Y. Yamada, *Appl. Phys. Lett.* **97**, 021906 (2010).
 [7] K. Takahashi, T. Kanno, A. Sakai, H. Adachi, and Y. Yamada, *Phys. Rev. B* **83**, 115107 (2011).
 [8] D. Sun, G. Aivazian, A. M. Jones, J. S. Ross, W. Yao, D. Cobden, and X. Xu, *Nat. Nanotechnol.* **7**, 114 (2012).
 [9] L. Prechtel, L. Song, D. Schuh, P. Ajayan, W. Wegscheider, and A. W. Holleitner, *Nat. Commun.* **3**, 646 (2012).
 [10] L. Prechtel, M. Padilla, N. Erhard, H. Karl, G. Abstreiter, A. Morral, and A. W. Holleitner, *Nano Lett.* **12**, 2337 (2012).
 [11] B. Ferguson and X.-C. Zhang, *Nat. Mater.* **1**, 26 (2002).
 [12] M. Tonouchi, *Nat. Photon.* **1**, 97 (2007).
 [13] C. A. Schmuttenmaer, *Chem. Rev.* **104**, 1759 (2004).
 [14] X.-C. Zhang, Y. Jin, T. D. Hewitt, T. Sangsiri, L. E. Kingsley, and M. Weiner, *Appl. Phys. Lett.* **62**, 2003 (1993).
 [15] P. Gu, M. Tani, S. Kono, K. Sakai, and X.-C. Zhang, *J. Appl. Phys.* **91**, 5533 (2001).
 [16] K. Liu, J. Xu, T. Yuan, and X.-C. Zhang, *Phys. Rev. B* **73**, 155330 (2006).
 [17] M. Tonouchi, M. Tani, Z. Wang, K. Sakai, S. Tomozawa, M. Hangyo, Y. Murakami, and S. Nakashima, *Jpn. J. Appl. Phys.* **35**, 2624 (1996).
 [18] K. Takahashi, N. Kida, and M. Tonouchi, *Phys. Rev. Lett.* **96**, 117402 (2006).
 [19] N. Kida and M. Tonouchi, *Appl. Phys. Lett.* **78**, 4115 (2001).
 [20] J. Maysonave *et al.*, *Nano Lett.* **14**, 5797 (2014).
 [21] P. A. Obraztsov, N. Kanda, K. Konishi, M. Kuwata-Gonokami, S. V. Garnov, A. N. Obraztsov, and Y. P. Svirko, *Phys. Rev. B* **90**, 241416(R) (2014).
 [22] K. Takahashi, T. Kanno, A. Sakai, H. Tamaki, H. Kusada, and Y. Yamada, *Adv. Opt. Mater.* **2**, 428 (2014).
 [23] K. Takahashi, T. Kanno, A. Sakai, H. Adachi, and Y. Yamada, *Cryst. Growth Design* **12**, 1708 (2012).
 [24] A. Bonvalet and M. Joffre, in *Femtosecond Laser Pulses: Principles and Experiments*, 2nd ed., edited by C. Rulliere (Springer, New York, 2004).
 [25] M. Yamashita, C. Otani, T. Matsumoto, Y. Midoh, K. Miura, K. Nakamae, K. Nikawa, S. Kim, H. Murakami, and M. Tonouchi, *Opt. Express* **19**, 10864 (2011).
 [26] G. Klatt *et al.*, *Opt. Express* **18**, 4939 (2010).
 [27] M. E. Barnes *et al.*, *Opt. Express* **20**, 8898 (2012).
 [28] M. E. Barnes, S. A. Berry, P. Gow, D. McBryde, G. J. Daniell, H. E. Beere, D. A. Ritchie, and V. Apostolopoulos, *Opt. Express* **21**, 16263 (2013).
 [29] X.-C. Zhang, B. B. Hu, J. T. Darrow, and D. H. Auston, *Appl. Phys. Lett.* **56**, 1011 (1990).
 [30] Y. Jin, X. F. Ma, G. A. Wagoner, M. Alexander, and X.-C. Zhang, *Appl. Phys. Lett.* **65**, 682 (1994).
 [31] K. Takahashi, A. Sakai, H. Adachi, and T. Kanno, *J. Phys. D: Appl. Phys.* **43**, 165403 (2010).
 [32] T. Kanno, S. Yotsuhashi, and H. Adachi, *Appl. Phys. Lett.* **85**, 739 (2004).
 [33] S. K. Sundaram and E. Mazur, *Nat. Mater.* **1**, 217 (2002).
 [34] N. L. Wang, P. Zheng, D. Wu, Y. C. Ma, T. Xiang, R. Y. Jin, and D. Mandrus, *Phys. Rev. Lett.* **93**, 237007 (2004).
 [35] M. D. Johannes, I. I. Mazin, and D. J. Singh, *Phys. Rev. B* **71**, 205103 (2005).
 [36] A. B. Focke and J. R. Hill, *Phys. Rev.* **50**, 179 (1936).
 [37] K. Fischer, C. Stoiber, A. Kyarad, and H. Lengfellner, *Appl. Phys. A* **78**, 323 (2004).
 [38] D. Boschetto, E. G. Gamaly, A. V. Rode, B. Luther-Davies, D. Glijer, T. Garl, O. Albert, A. Rousse, and J. Etchepare, *Phys. Rev. Lett.* **100**, 027404 (2008).